Molecular Therapy
Methods & Clinical Development
Original Article

OCT4 induces long-lived dedifferentiated kidney progenitors poised to redifferentiate in 3D kidney spheroids

Dorit Omer,[1,2] Osnat Cohen Zontag,[1,2] Yehudit Gnatek,[1,2] Orit Harari-Steinberg,[1,2] Oren Pleniceanu,[1,2] Michael Namestnikov,[1,2] Ayelet-Hashahar Cohen,[3] Malka Nissim-Rafinia,[3] Gal Tam,[4] Tomer Kalisky,[4] Eran Meshorer,[3,5] and Benjamin Dekel[1,2,6]

[1]Pediatric Stem Cell Research Institute, Edmond & Lily Safra Children's Hospital, Sheba Medical Center, Tel Hashomer 5262000, Israel; [2]Sagol Center for Regenerative Medicine, School of Medicine, Tel Aviv University, Tel Aviv, Israel; [3]Department of Genetics, The Alexander Silberman Institute of Life Sciences, The Hebrew University of Jerusalem, Edmond J. Safra Campus, Jerusalem 9190401, Israel; [4]Faculty of Engineering and Nanotechnology Institute, Bar-Ilan University, Ramat-Gan 5290002, Israel; [5]Edmond & Lily Safra Center for Brain Sciences (ELSC), The Hebrew University of Jerusalem, Edmond J. Safra Campus, Jerusalem 9190401, Israel; [6]Division of Pediatric Nephrology, Edmond & Lily Safra Children's Hospital, Sheba Medical Center, Tel Hashomer 5262000, Israel

Upscaling of kidney epithelial cells is crucial for renal regenerative medicine. Nonetheless, the adult kidney lacks a distinct stem cell hierarchy, limiting the ability to long-term propagate clonal populations of primary cells that retain renal identity. Toward this goal, we tested the paradigm of shifting the balance between differentiation and stemness in the kidney by introducing a single pluripotency factor, OCT4. Here we show that ectopic expression of OCT4 in human adult kidney epithelial cells (hKEpC) induces the cells to dedifferentiate, stably proliferate, and clonally emerge over many generations. Control hKEpC dedifferentiate, assume fibroblastic morphology, and completely lose clonogenic capacity. Analysis of gene expression and histone methylation patterns revealed that OCT4 represses the HNF1B gene module, which is critical for kidney epithelial differentiation, and concomitantly activates stemness-related pathways. OCT4-hKEpC can be long-term expanded in the dedifferentiated state that is primed for renal differentiation. Thus, when expanded OCT4-hKEpC are grown as kidney spheroids (OCT4-kSPH), they reactivate the HNF1B gene signature, redifferentiate, and efficiently generate renal structures *in vivo*. Hence, changes occurring in the cellular state of hKEpC following OCT4 induction, long-term propagation, and 3D aggregation afford rapid scale-up technology of primary renal tissue-forming cells.

INTRODUCTION

Current therapies for advanced chronic kidney disease (CKD) have major drawbacks. On the one hand, dialysis results in significantly reduced quality of life and does not replace all kidney functions. On the other hand, despite being the only alternative with curative potential, renal transplantation is seriously limited by eventually restricted graft survival and by the scarcity of donors.[1] A promising strategy that has been put forward in recent years as a potential alternative to conventional treatments is stem cell-based therapy. Accordingly, we previously defined a cell-surface biomarker system and prospectively isolated tissue stem/progenitors from human fetal kidneys that harbor renal potential and show regenerative capacities in experimental CKD.[2–4] Nevertheless, these represent an allogeneic cell source with the limitations of immunological barriers.[5,6] For autologous use, cells derived from human induced pluripotent stem cell (iPSC)-kidney differentiation or human adult kidneys are relevant.[7–9] For the adult kidney, *in vivo* clonal analysis and lineage tracing defined segmental boundaries for local regeneration.[10,11] These studies and recent single-cell RNA-sequencing studies of the adult kidney[12] indicate transitional cell states within segments that allow for cell replacement rather than hardwired professional stem/progenitors.[13,14] Therefore, the adult kidney lacks a distinct stem cell hierarchy, and this may limit the ability to long-term propagate clonal populations of primary cells that retain renal identity and renal potential.[6] Hence, cell expansion to clinically relevant numbers, which is a prerequisite for achieving a meaningful clinical effect, comes at the expense of *in vivo* renal identity/potential.[9] To exploit renal cell states that allow for *ex vivo* propagation of tissue-forming cells and maintenance of progenitor function as cells expand, 3D cultures of human kidney cells as spheroids and tubuloids have been formulated.[9] Kidney spheroids reestablish renal identity and function *ex vivo*, which translates into long-term engraftment and improved renal function in a mouse model of CKD.[9] Nonetheless, kidney spheroids by virtue of recapitulating the adult kidney have limited expansion capacity and can be mostly generated from adherent cells in relatively low passages (P0–P2).[9] In addition, tubuloids slowly expand

Received 6 April 2022; accepted 18 April 2023;
https://doi.org/10.1016/j.omtm.2023.04.005.

Correspondence: Benjamin Dekel, MD, PhD, Pediatric Stem Cell Research Institute & Division of Pediatric Nephrology, Sagol Center for Regenerative Medicine, Edmond & Lily Safra Children's Hospital, Sheba Medical Center, Tel Hashomer, Tel Aviv 5262000, Israel.
E-mail: binyamin.dekel@sheba.health.gov.il

and have not yet been shown to possess nephrogenic potential upon *in vivo* transplantation.[15] Indeed, to date, no data exist regarding stem/progenitor cells that can long-term clonally expand, upscaled in high passages (P5–P15), in a rapid manner and yet retain the capacity to generate renal tissue upon transplantation.[6,16]

Somatic cell reprogramming to pluripotent cells involves the forced expression of combinations of transcription factors associated with pluripotency together with selection for pluripotent cell growth in appropriate media.[17] In addition, alternative somatic fates that bypass the induced pluripotent cell stage were induced by initial transient expression of combinations of pluripotency transcription factors, including OCT4,[18,19] or by long-term expression of OCT4 alone followed by selective culture. Accordingly, OCT4 has been suggested as the gatekeeper into reprogramming that can be directed by altering the experimental conditions.[20] OCT4 is encoded by *POU5F1* and belongs to the family of Pou-domain transcription factors, and its expression is normally confined to pluripotent cells of the developing embryos, in which it plays a pivotal role in regulating self-renewal and pluripotency.[21] Intriguingly, it has been suggested that OCT4 may operate as a lineage specifier that leads to direct commitment to specific fetal lineages.[22] Such commitment was demonstrated upon OCT4 overexpression, terminating in mesodermal differentiation of embryonic stem cells.[23] Furthermore, in some somatic cells (other than the kidney) ectopic expression of OCT4 examined in a transgenic mouse model has been associated with active dedifferentiation.[24]

Hence, we hypothesized that introduction of OCT4 may result in shifting the balance between differentiation and stemness of primary human kidney epithelial cells (hKEpC). Herein, we show that ectopic expression of OCT4 (OCT4-hKEpC) dedifferentiates primary adult renal cells, allowing them to clonally expand over many generations. OCT4 represses the HNF1B-dependent renal cell differentiation program concomitant with activation of cell-cycle and stemness pathways to generate tissue progenitors primed for renal lineage maturation. Accordingly, high-passage OCT4-hKEpC cultured as 3D kidney spheroids (OCT4-kSPH) reactivate the HNF1B gene module, remature, and efficiently generate proximal tubule structures *in vivo*, allowing the establishment of long-lived tissue cells in a timely manner.

RESULTS

Ectopic expression of *OCT4* in human adult kidney epithelial cells results in long-term clonal expansion

We prepared adherent cultures from human renal cortical specimens that were derived from surgical nephrectomies.[9,25,26] We then attempted to ectopically express OCT4 in hKEpC preparations using lentiviral delivery. Mock-infected hKEpC of the same passage served as a control. Human *OCT4* was introduced simultaneous with a puromycin (Puro) resistance gene (Figure S1A). Cells were analyzed after 2–3 weeks. OCT4 immunofluorescence revealed strong nuclear staining, which could not be detected in mock-infected hKEpCs (Figures S1B and S1C). OCT4-induced cells underwent morphological changes, appearing as homogeneous clusters of small round cells (Figure 1A). The proliferative capacities of OCT4-hKEpC were then monitored *in vitro*. Remarkably, OCT4-hKEpC were proliferative in adhesion culture and could be expanded to high passages (P15) in the presence of serum while maintaining their homogeneous small round morphology, indicative of long-term self-renewal (Figure 1B). This is in sharp contrast to mock-infected controls, which proliferate to adopt a fibroblastic-like appearance upon passaging (Figure 1B). In contrast to control cells, which demonstrated an increase in doubling time along passages, OCT4-hKEpC maintained a stable proliferation rate, indicating a stable phenotype (Figure 1C). Chromosomal G-band analysis showed that OCT4-hKEpC retained a normal diploid karyotype, indicating that the cells did not undergo neoplastic transformation (Figure S1D). To exclude the possibility that OCT4-hKEpC have acquired a pluripotent phenotype, we injected iPSCs and OCT4-hKEpC into the peritoneal cavity of NOD/SCID mice. While control iPSCs formed teratomas (3/3 mice), OCT4-hKEpC failed to do so (0/6 mice, Fisher exact test, $p < 0.01$) (Figure S1E), excluding the acquisition of a pluripotent state and, in addition to that, tumorigenic transformation.

To demonstrate that the small round cell colonies of OCT4-hKEpC emerge from a single cell upon culture passage, we labeled cells with mCherry using a lentivirus-based vector devoid of antibiotic selection, enabling the formation of two cell populations, $mCherry^{POS}$-OCT4-hKEpC and $mCherry^{NEG}$-OCT-hKEpC. We observed red or colorless, but not mixed, colonies, indicating that clonal expansion underlies cell growth (Figure 1D). In addition, limiting-dilution and colony-forming-unit (CFU) assays demonstrated that control cells formed colonies only rarely, while OCT4-hKEpC showed significant colony-formation capacity (Figure 1E). Thus, induction of OCT4 in hKEpC allowed for clonal cell expansion. Since OCT4-hKEpC show clonal behavior over many passages, we were interested in determining whether a similar gene pattern is maintained across multiple single-cell clones that emerged from OCT4-hKEpC. Multi-gene expression analysis of six different clones demonstrated a similar gene profile with respect to epithelial-to-mesenchymal transition (EMT)-, cell-cycle-, and kidney-segment-related genes, suggestive of clonal homogeneity. Importantly, single-cell clones were also reminiscent of the total culture of OCT4-hKEpC and distinct from naive hKEpC (Figure 1F).

OCT4 induces dedifferentiation and stemness genes in hKEpC

Next, we queried the transcriptional changes that take place in hKEpC following OCT4 induction. OCT4-hKEpC were subjected to RNA-sequencing (RNA-seq) analysis and compared with mock-infected hKEpC from the same passage. Euclidean distance analysis separated OCT4-hKEpC from control samples, indicating distinct biological entities (Figure 2A). Analysis defined 1,841 genes as differentially expressed between OCT4-hKEpC and control samples. Gene set enrichment analysis (GSEA) of differentially expressed genes revealed upregulation of OCT4 targets (Figures S2A and S2B) and activation of EMT genes in OCT4-hKEpC (Figure 2B), including *SNAI2*, *THY1*, *CDH2*, *SOX9*, and *SMAD6*. Notably, fibroblast-related genes were not activated (*COL1A1*, *COL1A2*) or were downregulated

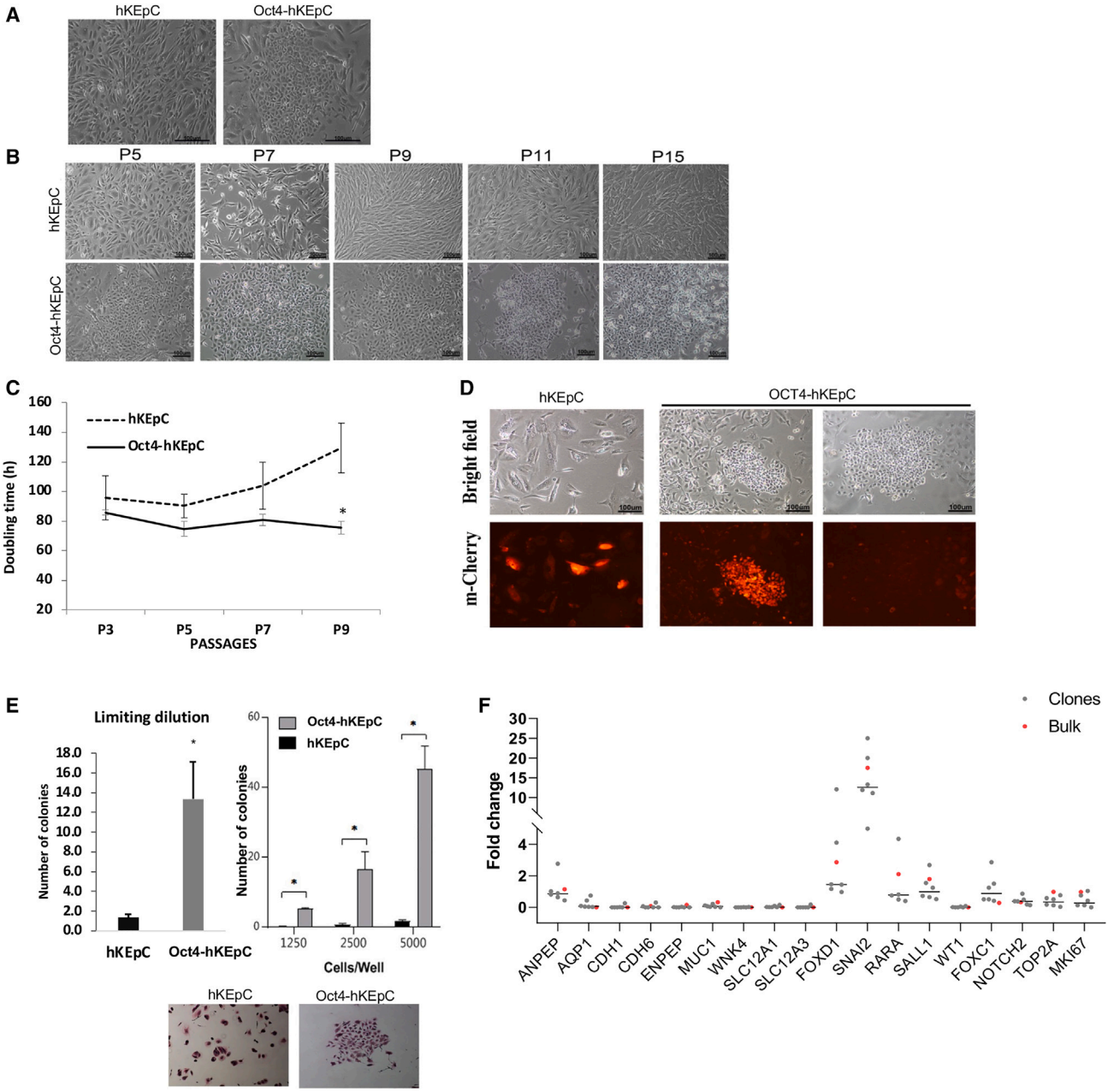

Figure 1. Overexpression of OCT4 in hKEpC

OCT4 overexpression in hKEpC was achieved via lentiviral infection (OCT4-hKEpC) carrying a puromycin-resistance cassette, and cells were selected by puromycin. Cells carrying an empty vector and a puromycin-resistance cassette served as control (hKEpC). (A) OCT4-hKEpC (right) undergo a phenotypic switch, appearing as a homogeneous cluster of small round cells. (B) OCT4-hKEpC maintained their round morphology through 15 passages, compared with control cells that had a spindle-shaped morphology (scale: 100 μm). (C) OCT4-hKEpC demonstrate a stable proliferation rate, whereas control cells exhibit an increased doubling time along passages. Data was calculated as average + SD, *p<0.05. (D) OCT4-hKEpC demonstrate clonal expansion, as manifested by the formation of two distinct types of colonies: mCherry^{POS}-OCT4-hKEpC and mCherry^{NEG}-OCT4-hKEpC (scale: 100 μm). (E) Top: OCT4-hKEpC are clonogenic at high passages (P5–P7), as seen in the limiting-dilution (left, Data was calculated as average + SD, *p>0.05) and colony-forming-unit (CFU; right, Data was calculated as average + SD, *p<0.005) assays. Bottom: Giemsa staining of control hKEpC- vs. OCT4-hKEpC-derived colonies. (F) OCT4-hKEpC-derived colonies showed a genetic profile similar to that of the bulk culture of OCT4-hKEpC (the total culture), as demonstrated by multi-gene expression analysis, both compared with naive hKEpC.

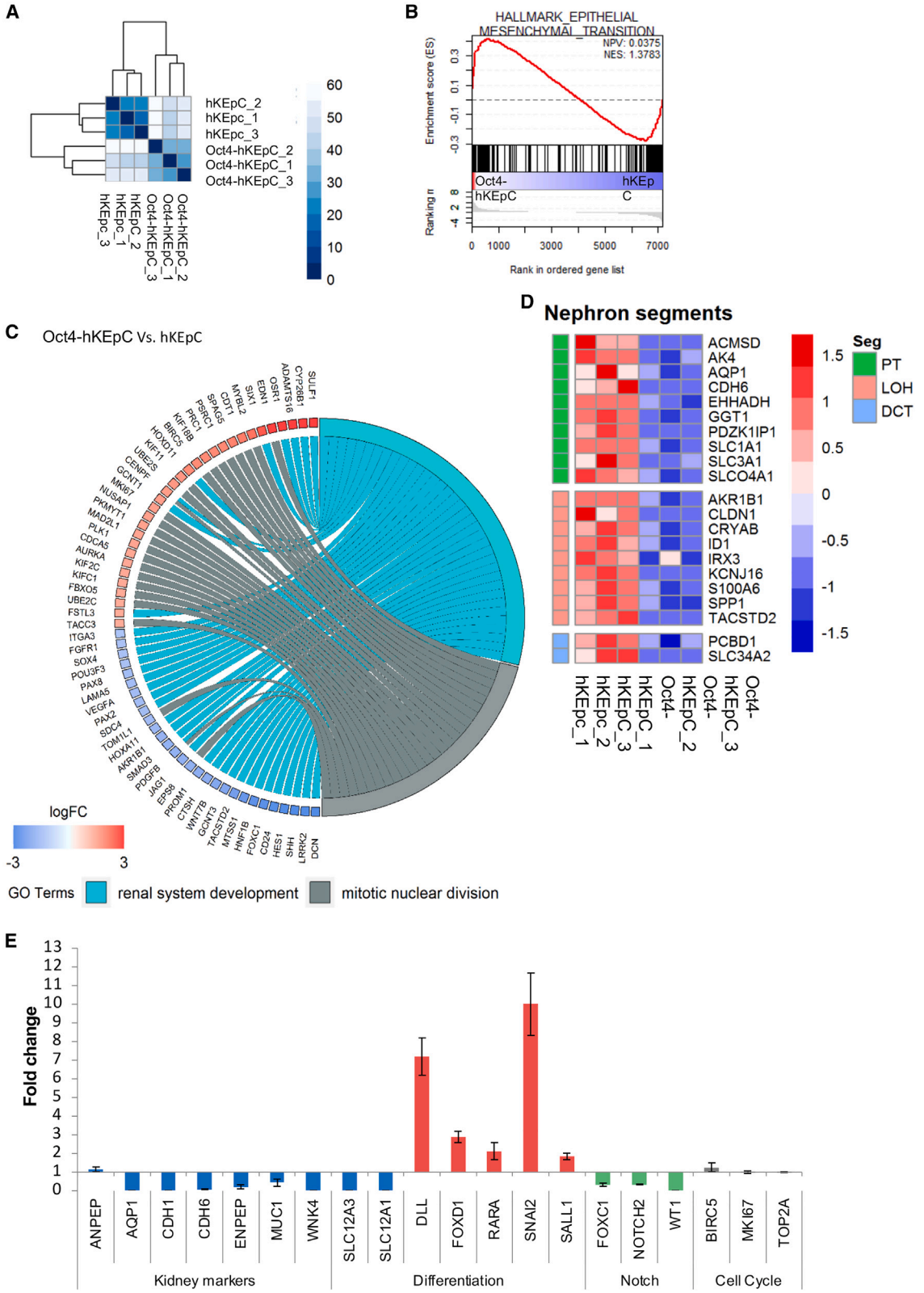

(legend on next page)

(*FN1*, *IL6*, *STAT6*, *S100A4* [*Fibroblast specific protein 1*], *CD9*), excluding EMT resulting in generation of fibroblasts (Figure S2C). This was accompanied by enhanced expression of key effectors of early renal mesenchyme and metanephric kidney development (*OSR1*, *SIX1*, *HOXD11*, *SULF1*, and *CYP26B1*)[27,28] (Figure 2C), as well as transcriptional regulators of mesenchymal progeny, including cardiac (*MEF2C*, *ISL1*, *VEGFC*)[29] and hematopoietic (*RUNX1*)[30] lineages. Consistent with this shift toward a more mesenchymal state, we noted a reduction in renal epithelial differentiation genes such as *LHX1*, *PAX2*, *PAX8*, *HNF1B*, and *JAG1* and renal epithelial markers (e.g., *SLC3A1*, *AQP1*, *CLDL1*, *CDH6*, *SLC34A2*, *CD24*) (Figures 2C and 2D). Overall, these changes suggest dedifferentiation in OCT4-hKEpC. In addition, OCT4-hKEpC displayed activation of genes related to the Wnt pathway (e.g., *FZD5*, *APCDD*, *TLE4*, *NDP*, *NLK*, *PTK7*), a developmental pathway that has been linked to the effects of progenitor cell induction and self-renewal by OCT4 in the mouse model.[31] Finally, consistent with their *in vitro* phenotype, genes associated with cell-cycle progression were upregulated in OCT4-hKEpC compared with control cells (Figures 2C and S2B). RNA-seq verification with qPCR analysis demonstrated dedifferentiation/EMT (downregulation of *E-cadherin* alongside induction of *Vimentin*) (Figure S2D), downregulation of kidney epithelial markers, and induction of early renal mesenchymal markers (*OSR1*, *SIX2*) (Figure S2D). Finally, to compare OCT4-hKEpC with native kidney cells, we analyzed high-passage OCT4-hKEpC and naive P0 hKEpC using multi-gene expression analysis. OCT4-hKEpC showed a decrease in Notch pathway-related genes; reduction in segment-specific molecules of all nephron segments (podocytes, loop of Henle, and distal tubule), apart from the proximal tubule marker CD13; and elevation of EMT genes[32] (Figure 2E). Remarkably, cell-cycle genes demonstrated similar expression levels in both cell types (Figure 2E). Thus, high-passage OCT4-hKEpC are stably proliferating in a dedifferentiated phenotype.

ChIP-seq of OCT4-hKEpC further delineates dedifferentiation and stemness pathways

To provide further molecular insight into the identity of OCT4-hKEpC, and since high numbers of chromatin-modifying genes were elevated in OCT4-hKEpC, we performed chromatin immunoprecipitation followed by high-throughput sequencing (ChIP-seq) analysis, focusing on two types of epigenetic modifications: the activity-related histone modification H3K4me3 and the suppressive polycomb-related histone modification H3K27me3 (Table S1). We also specifically analyzed genes exhibiting the "bivalent" mark comprising both H3K4me3 and H3K27me3, usually signifying genes with transcriptional potential, but with little or no expression (Table S1). These modifications were compared in OCT4-hKEpC vs. similar-passage naive hKEpC. We identified an overlap between the results of RNA-seq and ChIP-seq analysis; genes that were upregulated in RNA-seq were the genes marked with H3K4me3, and the downregulated genes were marked with H3K27me3 (Figure S3A). Importantly, known OCT4 targets showed a significant overlap with H3K4me3 modified genes only in OCT4-hKEpC, ascertaining the activation of OCT4 targets (Figure 3A). Consistent with the RNA-seq results, ontology analysis of the genes demonstrating H3K27me3 modification in OCT4-hKEpC revealed enrichment of epithelium development and, specifically, kidney epithelial and tubular development (Figure 3B), again corroborating with epithelial dedifferentiation demonstrated in the transcriptional analysis. When a similar analysis was performed on OCT4-hKEpC H3K4me3-modified genes, we noticed an enrichment in terms related to Wnt signaling, cell division, and chromatin organization (Figure 3B). Ontology analysis of the H3K4me3 modified known OCT4 targets concomitantly revealed enrichment in Wnt pathway, as well as somatic stem cell population maintenance (GO:0035019) (Figure 4C). Interestingly, analysis using the ChIP-Atlas software[33] revealed that the main regulators of the H3K27me3 modification in OCT4-hKEpC were the polycomb group members, EZH2 and JARID2, which belong to the PRC2 complex, previously shown to be involved in epigenetic regulation of many genes via the H3K27me3 modification[34] (Figure 3B). This was in accordance with their upregulated expression levels in OCT4-hKEpC shown in the RNA-seq analysis (Figure S3B).

OCT4 represses the HNF1B gene module in hKEpC

An intriguing observation was that HNF1B, a key regulator of renal epithelial differentiation,[35–37] whose inhibition is related to upregulation of SNAI2 and EMT,[38] was significantly repressed in OCT4-hKEpC according to RNA-seq data. Since HNF1B is known to be epigenetically repressed by EZH2,[39] we speculated that OCT4 induction might inhibit HNF1B expression via EZH2-mediated H3K27me3 modification. Indeed, overlapping analysis with known HNF1B targets and histone-modified genes from the ChIP-seq data revealed a significant overlap with H3K27me3 modification in OCT4-hKEpC and with H3K4me3 modification in naive cells, further indicating HNF1B pathway repression specifically in OCT4-hKEpC (Figure 3A). Consistent with the epigenetic analysis, HNF1B targets were also found to be downregulated in OCT4-hKEpC, including *PAX2, PAX8, JAG1,* and *LHX1*, confirming the inhibition of this pathway (Figure 3D). Interestingly, analysis using the ChIP-Atlas software[33] revealed that the main regulators of the H3K27me3 modification in OCT4-hKEpC were the polycomb group members, EZH2 and JARID2, which belong to the PRC2 complex, previously shown to

Figure 2. RNA-seq analysis of OCT4-hKEpC and hKEpC

(A) Euclidean distance analysis was performed on RNA-seq data to illustrate variation in transcription levels between OCT4-hKEpC and hKEpC. The distance between cell types is demonstrated by a heatmap. While OCT4-hKEpC are different from hKEpC, replicates are clustered together. Darker color indicates a smaller distance, which means greater similarity. (B) Gene set enrichment analysis (GSEA) shows upregulation of EMT-related genes in OCT4-hKEpC. (C) Gene ontology chord chart shows upregulation of early renal mesenchymal progenitors and metanephric kidney development and downregulation of renal epithelial developmental genes in OCT4-hKEpC compared with hKEpC together with upregulation in cell-cycle-progression genes. (D) OCT4-hKEpC show reduction in renal epithelial markers, suggesting renal epithelial lineage repression. (E) Comparison of high-passage (P5–P7) OCT4-hKEpC with naive P0 hKEpC, using multi-gene expression analysis.

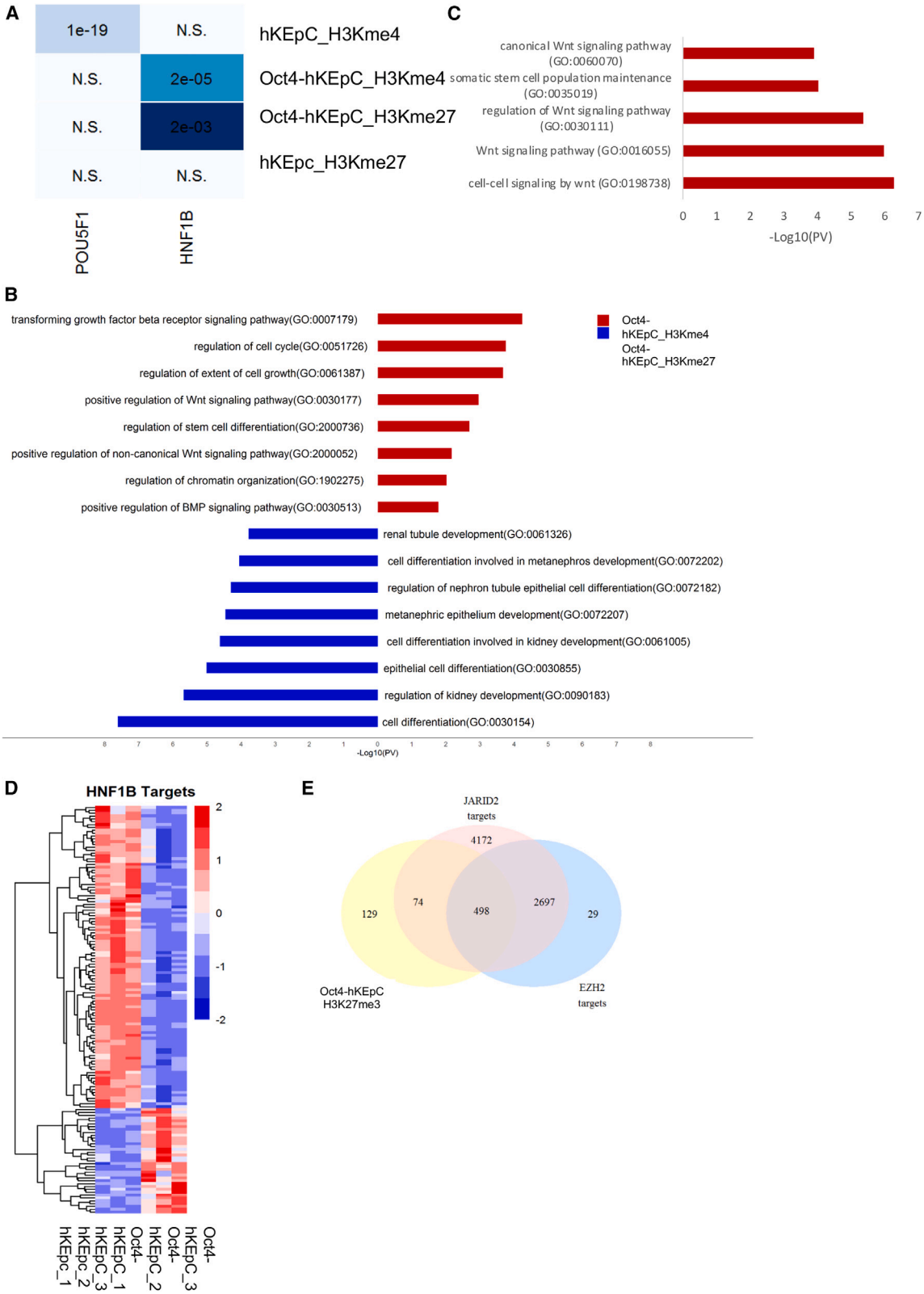

(legend on next page)

be involved in epigenetic regulation of many genes via the H3K27me3 modification[34] (Figure 3E). This was in accordance with their upregulated expression levels in OCT4-hKEpC shown in the RNA-seq analysis (Figure S3B). Last, when analyzing the group of genes marked by the H3K4me3/H3K4me27 signature,[40] we found that various genes related to kidney epithelialization (e.g., *CD24, WNT5B, GATA3, PAX2, RSPO2, LGR6*) are marked by a bivalent signature, typical of genes that are inactive but poised for activation and change in cellular state. This notion was supported by ontology analysis of poised genes in OCT4-hKEpC (Figure S3C).

Clonal OCT4-hKEpC retain functional traits *in vitro*

We next queried changes at the protein level. Fluorescence-activated cell-sorting (FACS) analysis demonstrated substantial reduction of renal epithelial differentiation markers CD24, CD133, and EpCAM.[4,26,41] The distal tubular marker EMA was not expressed in OCT4-hKEpC, whereas the proximal tubule marker CD13 was reduced but was still significantly expressed (Figures 4A and S4A). In addition, we found induction of the mesenchymal markers CD90 (THY-1)[42,43] and CD105 (Figures 4A and S4A). Since conversion of fibroblasts by long-term expression of OCT4 into an alternative somatic cell fate was associated with the appearance of the pan-hematopoietic marker CD45,[17] we analyzed its expression in OCT4-hKEpC and found it to be lacking (Figures 4A and S4A). Altogether, these results validate the dedifferentiated phenotype of OCT4-hKEpC. Similarly, immunostaining revealed that OCT4-hKEpC are negative for the epithelial marker cytokeratin and tubular markers LRP2, AQP1, EMA, and *Dolichos biflorus* agglutinin (DBA), whereas the proximal tubular markers CD13 and *Lotus tetragonolobus* lectin (LTL) were positive at moderate and low levels, respectively (Figure 4B), suggesting that dedifferentiated OCT4-hKEpC might have partially retained a proximal tubular identity.

OCT4-hKEpC integrate into grafts of human fetal kidney but show limited tubulogenic potential

To delineate aspects of the *in vivo* potential of OCT4-hKEpC, we developed an assay to analyze their fate in a milieu of human fetal kidney cells (hFKCs). Clonal OCT4-hKEpC were labeled with the fluorescent marker cmDil and co-grafted with hFKCs at a ratio of 1:2 (respectively) in NOD/SCID mice (Figure 5A). Analysis at day 14 showed that hFKCs were able to integrate (Figure 5B) into hFKC-derived tubules as single cells or extended tubular portions (Figure 5B). Importantly, control hKEpC failed to integrate into hFKC-derived renal tubules. Moreover, we noticed that the number of hFKC-derived structures was higher when hFKCs were co-grafted with OCT4-hKEpC compared with co-grafting of hFKC with hKEpC or when grafted alone, suggesting that OCT4-hKEpC might induce hFKC tubulogenesis (Figure 5C). Thus, high-passage (P7–P10) OCT4-hKEpC harbor *in vivo* integration potential. We next analyzed the renal differentiation potential of OCT4-hKEpC upon grafting into adult hosts. To this end, we performed a series of transplantation assays of high-passage OCT4-hKEpC alongside control hKEpC into NOD/SCID mice (Figure 5D). For detection of the xenografted human cells, we used human leukocyte antigen (HLA) and renal epithelial markers that were tested on human adult kidney tissue (Figure S4B). OCT4-hKEpC and hKEpC were analyzed 14 days post-transplant. At day 14, OCT4-hKEpC were seen to form non-organized cell aggregates and more organized, albeit immature-appearing, HLA^+ structures. Notably, these were devoid of polarity and showed a low-level degree of self-organization. In contrast, control passage-matched hKEpC did not establish any structures, showing complete lack of renal potential (Figures 5E, 5F, and S4C). Importantly, OCT4 was detected in cell aggregates but was devoid of renal structures (Figures 5E and 5F), indicating that OCT4 may actively inhibit renal epithelial differentiation when OCT4-hKEpC are directly xenotransplanted into mice. Moreover, we observed that, parallel to the loss of OCT4 expression, cells within organizing structures reacquired cytokeratin expression that was lost in cultured OCT4-hKEpC (Figure 5G). Analysis of renal segment identity of grafted OCT4-hKEpC using renal epithelial markers showed that the few established structures were positive for LTL, CD13, and AQP1, indicative of a proximal nature (Figures 5H–5J).

Culturing of long-term-expanded *OCT4*-hKEpC as 3D kidney spheroids leads to redifferentiation

Having observed the limited *in vivo* renal potential of OCT4-hKEpC, we reasoned that growth of OCT4-hKEpC as 3D kSPH[9] may circumvent this limitation. We recently demonstrated that, once transferred from 2D to 3D culture conditions using serum-free medium (N2 and B27 supplemented), adult kidney cells undergo reepithelization (Figure S4D).[9] Utilizing our optimized protocol for 3D kidney cell growth we first established that high-passage OCT4-hKEpC (P7–P10) can be cultured as 3D kSPH (OCT4-kSPH) (Figure S6A). We then queried the OCT4 status in OCT4-kSPH and found significantly reduced OCT4 levels (Figure S5A). RNA-seq analysis of OCT4-kSPH showed that, concomitant to *OCT4* reduction, EMT (Figure 6B) and cell-cycle genes were downregulated, while renal epithelial differentiation genes (Figures 6C, S5A, and S5B), renal epithelial markers (Figure 6D), and renal tubule transporters (Figure S5C) were upregulated. Remarkably, OCT4-kSPH show activation of HNF1B and its targets, the opposite of OCT4-hKEpC grown in monolayer, indicating renal lineage derepression (Figure S5Di). Co-staining of the OCT4-kSPH for the

Figure 3. ChIP-seq analysis of OCT4-hKEpC and hKEpC

(A) Overlapping analysis between the known targets of OCT4 (POU5F1) and HNF1B with H3K4me3- and H3K27me3-modified genes in OCT4-hKEpC and in hKEpC. Colors represent odds ratio, numbers represent p value; N.S., non-significant overlap. (B) Ontology analysis of H3K4me3- (red) and H3K27me3- (blue) modified genes in OCT4-hKEpC. Analysis was performed with citrome-GO software. Only genes found to be exclusively modified in OCT4-hKEpC and not in hKEpC were analyzed. (C) Ontology analysis of known OCT4 target genes that were found to have H3K4me3 modification in OCT4-hKEpC. (D) Heatmap representation of known HNF1B targets that are differentially expressed in OCT4-hKEpC in comparison with hKEpC according to RNA-seq analysis. Most HNF1B target genes are downregulated in OCT4-hKEpC. (E) Venn diagram represents intersection of H3K27me3-modified genes in OCT4-hKEpC with the gene targets of EZH2 and JARID2, part of the PRC2 complex.

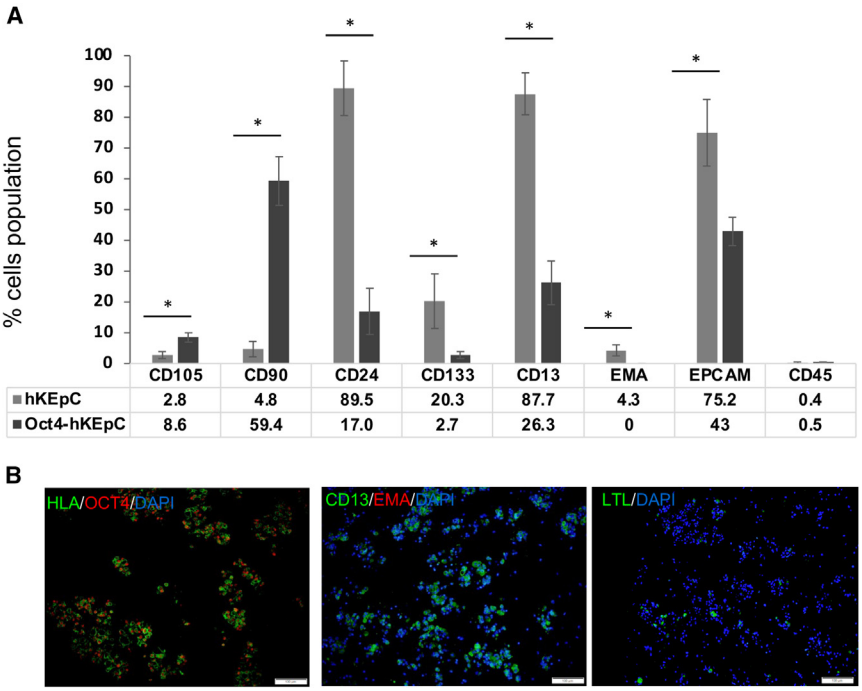

Figure 4. Clonal OCT4-hKEpC maintain renal identity

(A) FACS analysis of mesenchymal markers (CD90 and CD105), markers of cultured kidney epithelial cells (CD24 and CD133), markers of specific kidney nephron segments (CD13 and EMA), and a hematopoietic marker (CD45), Data was calculated as average + SD, *p<0.05. (B) Immunofluorescent staining of OCT4-hKEpC demonstrates tritest of proximal tubule phenotype, CD13, and LTL (scale 100 μm).

proximal tubule marker LTL and HNF1B demonstrated that the two markers are co-expressed, supporting that HNF1B drives redifferentiation of the cells (Figure S5Dii). Immunostaining of OCT4-kSPH showed expression of the renal epithelial markers cytokeratin, LTL, EMA, and AQP1 (Figure 6E). In addition, comparison of the expression ratio of nephron segment marker genes in OCT4-kSPH revealed prominent elevation of proximal tubule genes (Figure 6F), while GO analysis demonstrated elevation in fatty acid oxidation and mitochondrial activity characteristic of proximal tubule function (Figures 6F and 5SE, and Table S2).[44–46] GO analysis of differentially expressed (DE) genes in OCT4-hKEpC and OCT4-kSPH, both compared with control samples, identified that GO terms related to cell cycle enriched in genes upregulated in OCT4-hKEpC were downregulated in OCT4-kSPH. GO terms related to kidney development and cell adhesion were enriched in genes that were downregulated in OCT4-hKEpC and upregulated in OCT4-kSPH (Figure S6A). To further characterize the effect of OCT4 induction, we compared all samples with kidney organoids derived from iPSCs and from adult tissues by Euclidean distance analysis. OCT4-hKEpC were clustered with iPSC kidney organoids that represent an early kidney developmental stage, while the rest of the samples were clustered together (Figure S6B).

Redifferentiated OCT4-kSPH generate renal structures *in vivo*

We next tested whether molecular changes observed in OCT4-kSPH would lead to enhanced renal potential. We grafted high-passage (P7–P10) OCT4-kSPH into murine hosts and followed their engraftment pattern. Remarkably, we now found significant renal differentiation into mature renal structures, which was not observed when employing OCT4-hKEpC (Figure 7A). Notably, a comparison with control kSPH generated from low-passage hKEpC (P1-hKEpC-kSPH) and with fresh naive hKEpC showed the development of similar renal structures *in vivo* (Figure 7A), while, as mentioned above, high-passage (P7–P10) hKEpC-kSPH failed to generate renal structures (Figure S7A). Moreover, when comparing high-passage OCT4-kSPH with passage-matched hKEpC cultured as spheroids, a significantly higher number of renal structures was observed in the former (Figures S7B and S7C). Analysis of the human renal structures of post-transplant high-passage OCT4-kSPH revealed a proximal tubular phenotype, characteristically positive for CD13, LRP2 (megalin), AQP1, and LTL (Figures 7B and S7D), but negative for markers of distal tubules (E-cadherin and EMA), collecting ducts (AQP2), and podocytes (PODXL). Similar structures were developed from low-passage hKEpC-kSPH[9] (Figure 7C), but phenotypically, the latter expressed both distal and proximal markers (Figure 7C). Thus, it was established that OCT4-kSPH can be used as a means to preserve the *in vivo* renal potential of cultured renal cells even after long-term culture.

DISCUSSION

In the present study, we generated OCT4-induced hKEpC. OCT4-hKEpC clonally emerge and actively proliferate in a dedifferentiated state over many culture generations, affording large cell quantities. Importantly, OCT4-hKEpC are primed toward kidney differentiation, so that once cultured as 3D kSPH, long-term expanded OCT4-hKEpC redifferentiate to become more quiescent, regain epithelial identity, and show robust renal potential in transplantation assays. Therefore, this two-step strategy afforded by changes in cellular state is suitable for the generation of practically unlimited numbers of tissue-forming cells in a timely manner, which could greatly benefit regenerative medicine.

Comparison of OCT4-hKEpC with control primary kidney cells shows striking differences. Control primary cultures proliferate and dedifferentiate along passages but, at the same time, assume a fibroblastic morphology, lose clonogenicity and renal potential (even if cultured as 3D kSPH), and ultimately reach senescence. In contrast, while dedifferentiation is the rule in OCT4-hKEpC cultures, stemness is gained following OCT4 induction with the appearance of long-lived

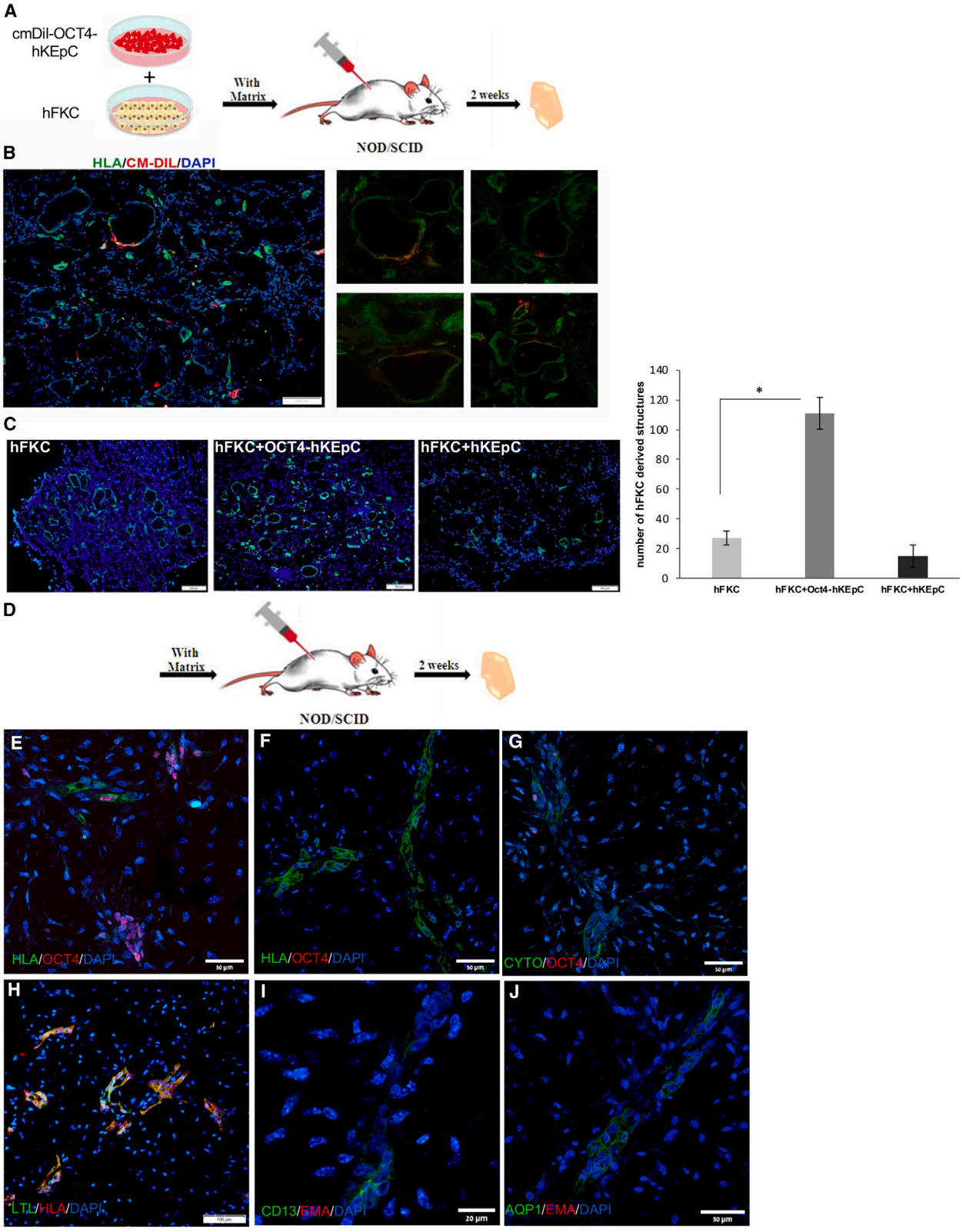

(legend on next page)

clones displaying homeostatic expansion and stable replication time, normal karyotype, and no evidence for tumorigenicity. We therefore can discern between abortive dedifferentiation appearing in expanded control primary cultures and "stemness-gained" dedifferentiation appearing in long-lived OCT4-hKEpC cultures. Importantly, previous attempts to induce long-term clonogenic proliferation in primary human kidney cultures via epigenetic modification with agents such as valproic acid and TSA (Trichostatin A) failed, and these agents induced senescence.[47]

We combined transcriptomics and analyses of global histone modification patterns and protein markers to comprehensively define OCT4-hKEpC. All data corroborate to show dedifferentiation of OCT4-hKEpC and transit to a more mesenchymal state, including activation of transcription factors marking early renal mesenchyme (*OSR1*, *SIX1*, *HOXD11*, *SULF1*, and *CYP26B1*). Bioinformatic analysis integrating transcriptomics with H3Kme4 (activation) and H3kme27 (repression) histone alterations suggests the interaction of OCT4 with HNF1B, a major renal epithelial differentiation transcription factor, leading to downregulation of the HNF1B gene module and hence renal epithelial dedifferentiation. Finally, stemness-related pathways were activated in OCT4-hKEpC, of which the Wnt pathway, previously shown to mark clonal kidney cell growth *in vivo*[10] and a well-established pathway crucial for tissue stem cell self-renewal,[48] was noted.

We employed two types of transplantation assays for *in vivo* analysis of renal potency of long-term expanded OCT4-hKEpC. The first utilized transplants of human fetal kidney tissue in NOD/SCID mice and analysis of the cells' integration potential in these developing grafts. The second entailed transplantation of human cells in Matrigel into the subcutaneous (SC) space of NOD/SCID mice and analysis of renal differentiation and structure formation. These assays suggested that, while OCT4-hKEpC harbor the capacity to integrate into the developing kidney grafts, they lack a robust capacity to differentiate and self-organize into renal structures in the SC assay. Previously, we described 3D culture conditions that allow for monolayers, which quickly decline in their renal potential, to form 3D kSPH. kSPH cultures transition to a more mature epithelial phenotype and enhance *in vivo* renal potency.[9,26,49] We reasoned that culturing of high-passage OCT4-hKEpC (P5–P10) as kSPH (OCT4-kSPH) may follow similar characteristics. Preservation of a partial renal epithelial phenotype in OCT4-hKEpC (i.e., LTL and CD13) and the existence of bivalent histone marks (H3Kme4/H3Kme27) on genes related to kidney epithelialization (*PAX2, GATA3, CD24, ALD1A2*) indicated that OCT4-hKEpC are likely to be primed for epithelial redifferentiation. Indeed, the transcriptomic shift between high-passage OCT4-hKEpC and OCT4-kSPH, best exemplified using cluster analysis, placed OCT4-hKEpC next to iPSC-derived kidney organoids, which harbor a fetal phenotype, while OCT4-kSPH were placed next to kSPH developed from primary renal cells and adult kidney organoids/tubuloids.[15,50] Notably, analysis of high-passage OCT4-kSPH using RNA-seq and analysis of gene and protein markers disclosed OCT4 reduction, reactivation of the HNF1B gene module, and establishment of renal epithelial markers. Since HNF1B is a critical determinant of tubule transport function by acting upstream of a large number of solute carrier (SLC) genes,[51] their expression can be instantly reestablished. These data may imply transcriptional epigenetic memory, in which renal epithelial marker genes remain poised for faster reactivation once a reduction in OCT4 levels occurs.[52] Closer examination of OCT4-kSPH demonstrated predominant upregulation of proximal tubule markers both on a global scale and with specific markers, correlating with the remnant proximal phenotype in OCT4-hKEpC (see above). The observation that a proximal tubule cell phenotype is preferentially expanded can be assigned to preferential infection of proximal cells in the heterogeneous culture. Alternatively, there may be *trans*-differentiation of distal toward proximal phenotypes. Understanding this phenomenon is beyond the scope of this article. Concomitantly, this cell phenotype developed in high-passage OCT4-kSPH, also correlated with the appearance of renal tubular structures of proximal nature (expressing CD13, LTL, AQP1, and LRP2) in transplantation assays. Importantly, primary renal cells expanded into high passages and grown as kSPH lack renal potency upon transplantation. Thus, long-lived OCT4-hKEpC grown as kSPH were exclusive in their *in vivo* capacities, matching freshly isolated kidney cells. Thus, this two-step dedifferentiation-redifferentiation method affords a unique cell source allowing unlimited upscaling in a timely manner to any passage required (as OCT4-hKEpC) and at the same time producing functional differentiated cells suitable for transplantation when shifted to 3D growth. This might be of practical importance when utilizing particularly small kidney biopsies from CKD patients for expansion of autologous cells or when rescuing and deriving primary renal cells from urine. While OCT4 levels are diminished in 3D kSPH, allowing redifferentiation, the mechanism of action responsible for OCT4 downregulation was not elucidated. We hypothesize that the changes in gene expression resulting from different culture conditions altered the regulation of the constitutive promotor of OCT4 ectopic gene (E1F promotor).

Figure 5. OCT4-hKEpC integrate into hFKC-derived tubules

(A) Scheme: OCT4-hKEpC or control-hKEpC were labeled with the fluorescent marker cmDil (red) and co-grafted with hFKC (not labeled) at a ratio of 1:2 (respectively) into NOD/SCID mice. The grafts were analyzed 2 weeks post-implantation. (B) OCT4-hKEpC both integrated into hFKC-derived tubular structures, seen as red cells within green (HLA^+) structures, and formed structures composed solely of OCT4-hKEpC (all cells are red), scale 100 μm. (C) Left: representative areas of grafts derived from each cell combination stained for HLA (green). Right: the number of hFKC-derived structures was higher when hFKCs were co-grafted with OCT4-hKEpC compared with co-grafting with control-hKEpC or when grafted alone, Data was calculated as average + SD, *$p<0.05$. (D) OCT4-hKEpC or hKEpC (P7–P10) were injected subcutaneously within Matrigel into NOD/SCID mice. Cell grafts were removed and analyzed after 14 days. (E–J) At day 14, OCT4-hKEpC, but not control-hKEpC, organized into immature structures or cell aggregates, while downregulating OCT4 expression. The structures demonstrate an epithelial proximal tubule phenotype, as manifested by the expression of cytokeratin, CD13, LTA, and AQP1 (scale: E–G, J- 50 μm, H- 100 μm, I- 20 μm).

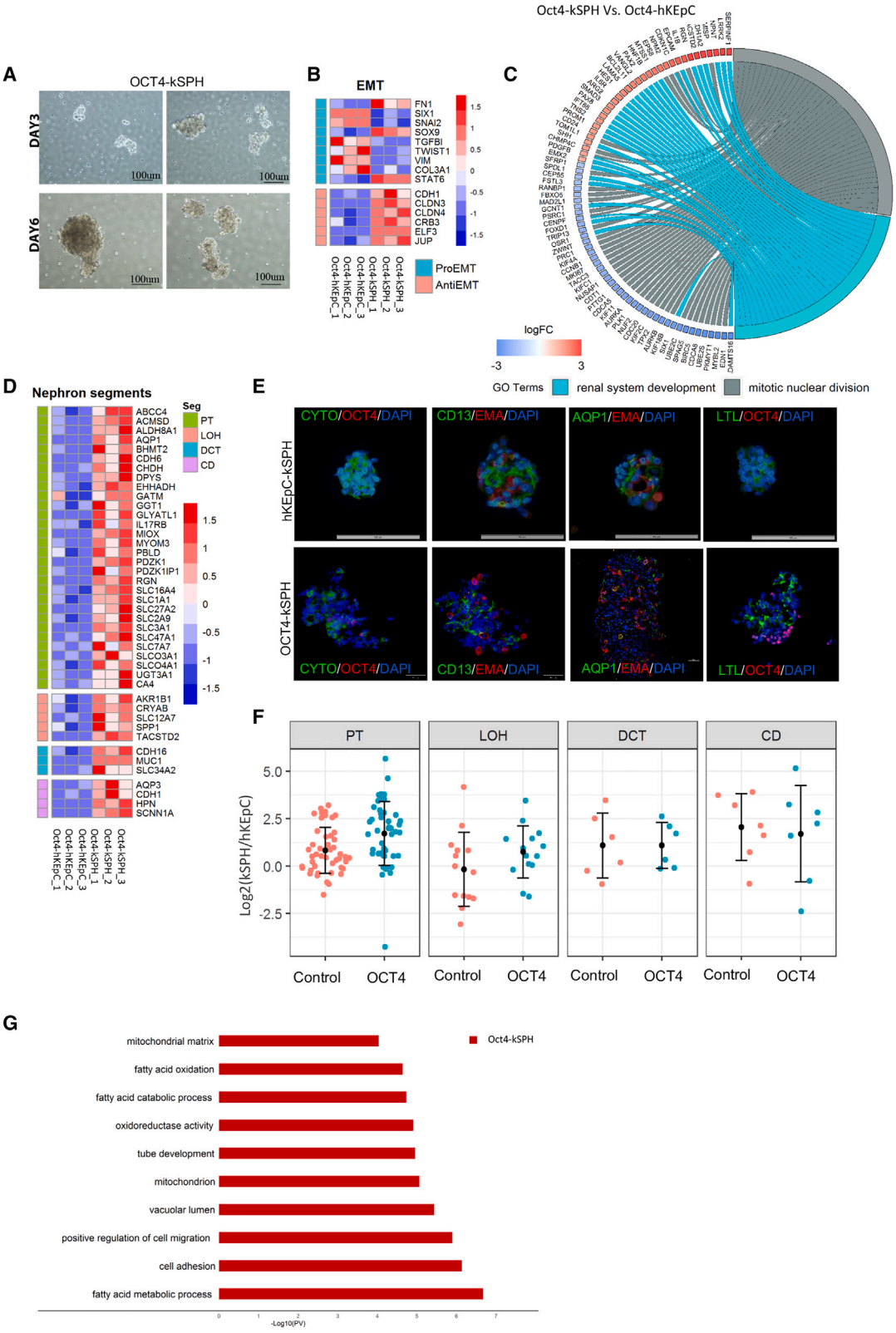

(legend on next page)

The recently described 3D human adult kidney epithelial tubuloids/organoids afford long-term expansion of functional adult tissue cells.[15] Nevertheless, long-lived tubuloids have not been assessed for *in vivo* potential. Moreover, their slowly proliferating nature may stand in the way of obtaining high cell numbers for scale up in a reasonable time frame. Other alternatives include studies reporting the generation of a mesenchymal nephron progenitor from a proximal tubule cell line by means of introducing serial embryonic renal transcription factors[53] or *trans*-differentiation of fibroblasts into proximal tubules using renal epithelial differentiation.[54] These, however, did not show long-term expansion of the established cell types nor *in vivo* renal capacities.

Finally, our combined approach may serve as a proof of principle for upscaling primary cells derived from epithelial tissues in a timely manner by manipulating the cell state. While the results of this study are compelling, they do carry risks to translation because of the usage of a vector technology. The use of non-viral approaches for cell expansion utilizing OCT4-modified mRNA is likely to be more relevant for regenerative medicine.

MATERIALS AND METHODS

Tissue samples

Human tissue samples were collected in accordance with the principles of the Declaration of Helsinki. Normal adult renal cortical tissues were retrieved from borders of renal cell carcinoma (RCC) tumors from partial nephrectomy patients at Sheba Medical Center, Tel Hashomer, Israel, and Wolfson Medical Center, Holon, Israel. All studies were approved by the local ethical committee and informed consent was given by the legal guardians of the patients involved, according to the Declaration of Helsinki.

Establishment of primary cultures from human kidney tissues

Human kidney samples were retrieved from the borders of RCC tumors resected from partial and total nephrectomy patients. Collected tissues were washed with PBS, weighed, and minced into ~1 mm slices using sterile surgical scalpels. The dissected tissue was then incubated for 2 h at 37°C with Iscoves' modified Dulbecco's medium (IMDM) (Invitrogen) supplemented with 0.1% collagenase IV (Invitrogen). The digested tissue was sieved through 100 μm cell strainers to achieve a single-cell suspension. The medium was removed by centrifugation and the cells were resuspended in growth medium and plated on gelatin-coated T175 flasks. Serum-containing medium (SCM) comprised IMDM (Biological Industries) supplemented with 10% fetal bovine serum (FBS; Invitrogen), 1% Pen-Strep 100 M and 1% L-glutamine (both purchased from Biological Industries), and 100 ng/mL EGF, 100 ng/mL bFGF, and 10 ng/mL SCF (all growth factors were purchased from Peprotech Asia). Cells were detached using 0.05% trypsin/EDTA (Invitrogen) upon reaching confluency and cryopreserved in 10% DMSO FBS. Two-dimensional hKEpC were photographed using Nikon Eclipse TS100 and Nikon Digital Sight cameras.

OCT4 overexpression

TransIT-LT1 transfection reagent (Mirus) was applied following the manufacturer's instructions to allow for transfection of HEK293 cells with pSin-EF2-*OCT4*-Pur vector (Addgene; retroviral vector expressing *OCT4* and puromycin resistance), control vector, and pSin-EF2-Pur vector (retroviral vector expressing puromycin resistance). Medium was aspirated after 8 h and fresh medium was provided. Two days post-transfection, supernatants of transfected cells filtered through a 0.45-μm-pore-size filter, and supplemented with Polybrene (hexadimethrine bromide; Sigma; 8 μg/mL final concentration). These viral preparations were used to infect hKEpC for 6 h, after which fresh medium was added. This infection procedure was repeated again the next day. Cells were selected 3 days post-infection for puromycin resistance (1.5 μg/mL).

kSPH formation

hKEpC or OCT4-hKEpC were grown as 2D cultures; upon reaching confluency of 80%–100%, the cells were harvested and seeded on poly(2-hydroxyethylmethacrylate) (poly-HEMA; Sigma-Aldrich)-precoated plates, in serum-free medium (SFM), at a concentration of 5.5–13 $\times$ 10^4 cells/mL. SFM comprised N2 medium (Biological Industries) supplemented with 1% Pen-Strep 100 M, 1% L-glutamine, 0.4% B27 supplement (Gibco); 4 μg/mL heparin sodium (Intramed); 1% non-essential amino acids, 1% sodium pyruvate, 0.2% CD lipid concentrate (all purchased from Invitrogen); 2.4 mg/mL glucose, 0.4 mg/mL transferrin, 10 mg/mL insulin, 38.66 μg/mL putrescine, 0.04% sodium selenite, 12.6 μg/mL progesterone (all from Sigma-Aldrich); and 10 ng/mL FGF and 20 ng/mL EGF. kSPH were photographed using Nikon Eclipse TS100 and Nikon Digital Sight cameras. After 7–10 days in culture, kSPH were collected and dismantled by incubation with TrypLE (GIBCO) for 10 min. kSPH-derived cells were then counted for further experimentation. For generating agarose blocks and RNA, medium with 2 million kSPH cells was collected and centrifuged and the kSPH pellet was retrieved.

Clonogenicity assays

Colony-forming-unit assay

hKEpC (control) or OCT4-hKEpC were plated on six well plates coated with Matrigel (R&D) at three different densities: 5,000,

Figure 6. OCT4-hKEpC show reepithelization when grown as spheroids (OCT4-SPH)

(A) Kidney spheroids derived from OCT4-hKEpC (OCT4-kSPH) (P7–P10) at days 3 and 6. (B) RNA-seq analysis shows reepithelization in OCT4-kSPH as evident by upregulation of anti-EMT genes. (C and D) OCT4-kSPH show the opposite trend of gene expression compared with OCT4-hKEpC: upregulation of early epithelial genes and reduction of cell-cycle genes and renal epithelial markers. (E) Immunofluorescent staining of hKEpC-kSPH and OCT4-kSPH. OCT4-kSPH show low expression of OCT4 and expression of renal epithelial markers: cytokeratin, CD13, EMA, AQP1, and LTL, scale: 100 μm. (F) Log2 fold change ratio of nephron segment marker genes between 2D and 3D cultures in hKEpC (control) (red) and OCT4-hKEpC (cyan) samples. Each dot represents one gene. Elevation in the expression level of proximal tubule (PT) and collecting duct (CD) markers in both control and OCT4 samples is seen. (G) Ontology analysis of genes with elevated expression level in OCT4-kSPH in comparison with OCT4-hKEpC.

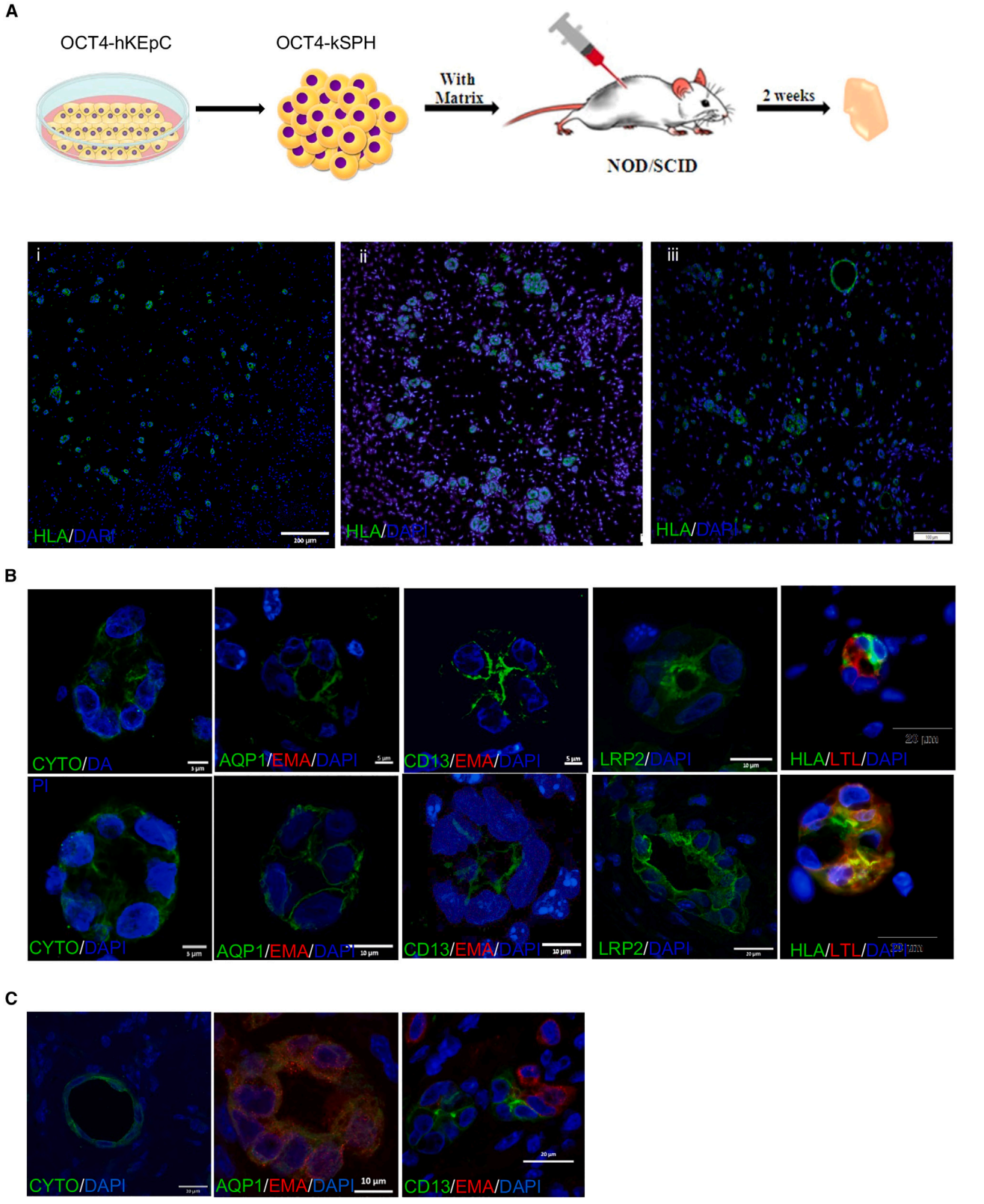

(legend on next page)

2,500, and 1,250 cells/well. Evaluation of colony formation was performed by Giemsa staining.

mCherry-marked colonies

Cells were first infected with *OCT4* or with control vector, both endowing puromycin resistance. A few days after selection, the cells were infected with an mCherry vector lacking a resistance gene to any antibiotic, enabling the formation of two cell populations, $mCherry^{POS}$ OCT4-hKEpC and $mCherry^{NEG}$ OCT4-hKEpC.

Agarose block preparation

Two million OCT4-hKEpC-, hKEpC-, or kSPH-derived cells were washed with PBS, fixed with 4% paraformaldehyde (PFA) for 2 h, washed again with PBS, and suspended in 200 μL of 2% UltraPure low-melting-point agarose (Invitrogen) (in 5% sucrose). Agarose with cells was then molded (the wide edge of a 1 mL tip was cut and used as a mold), fixed with 4% PFA overnight, and paraffin embedded.

Immunofluorescence staining

Five micrometer paraffin sections were pretreated with OmniPrep solution (pH 9.0) at 95°C for 1 h in accordance with the manufacturer's protocol (Zytomed Systems). Blocking was done using Cas-Block solution (Invitrogen immunodetection kit; 00-8120) for 1 h followed by 1 h incubation with two of the following primary antibodies: anti-OCT4 (Ms [Mouse]; Santa Cruz), anti-HLA (Rb [Rabbit] abcam) anti-cytokeratin (Dako, Glostrup Denmark), anti-LRP (Rb; Novus), biotinylated LTL (Vector Laboratories, Burlingame, CA), biotinylated DBA (Vector Laboratories, Burlingame, CA), anti-EMA (Ms; 1/2 of the prediluted antibody; Cell Marque; 247M-98), anti-CD13 (Rb, 1/400; abcam; 108382), anti-CD31 (Rb, 1/100; abcam; 28364), anti-Aqp1QP1 (Rb, 1/1,000; abcam; 168387), anti-AQP2 (Rb; abcam), anti-E-CAD (Rb; abcam), anti-PODXL (Rb; abcam), HNF1B (Rb; MERCK). Detection was done using Alexa Fluor 488-conjugated anti-rabbit and Alexa Fluor 555-conjugated anti-mouse secondary antibodies (Invitrogen) for 60 min. Mounting medium containing DAPI (Dapi Fluoromount-G; SouthernBiotech; 0100-20) was applied. Slides were analyzed using an Olympus BX51 fluorescence microscope and Olympus DP72 camera or a confocal microscope (ZEISS LSM700). Photo analysis was done using ZEN software.

Flow cytometry

Cells (0.5×10^5) were suspended in FACS buffer (0.5% BSA in 1× PBS). The cells were then incubated with a primary antibody or an isotype control (summarized above; antibodies as previously described in Harari-Steinberg et al.[9]). Cell viability was tested using 7AAD viability staining solution (eBioscience). Cell labeling was detected using FACSCalibur (BD Pharmingen). Flow cytometry results were analyzed using FlowJo analysis software (version 7.6.5).

Quantitative reverse transcription-PCR (qRT-PCR)

Total RNA was prepared using a Direct-zol RNA MiniPrep kit (Zymo Research) according to the manufacturer's instructions. Quantitative real-time PCR was done as previously described.[55] TaqMan gene expression primers and probes were purchased from Thermo Fisher Scientific.

Microfluidic multiplexed qRT-PCR

Total RNA was purified from individual clones derived from OCT4-hKEpC. Expression levels of preselected genes were measured by microfluidic multiplexed qRT-PCR (Fluidigm, South San Francisco, CA) with 18 cycles of preamplification as previously described.[56–58] This resulted in gene expression values (measured in threshold cycles; Ct) for each clone. We analyzed RNA from six clones with four technical replicates each, as well as two additional controls: RNA from OCT4-hKEpC culture and naive hKEpC (passage 1) with six technical replicates each. qPCR standard curves were created using serial dilutions of total RNA purified from cultured cells derived from adult and fetal kidney. We chose only the subset of genes for which the measured Cts were within the linear regime of the standard curves.

Data analysis

Data analysis was performed with MATLAB (Mathworks, Natick, MA). We first discarded reactions that did not work properly, identified as those for which the "housekeeping" gene GAPDH was not expressed. To normalize the Cts for the amount of RNA that was inserted for each sample, we used the housekeeping gene GAPDH as an internal control gene and subtracted its threshold cycle (Delta Ct = Ct − Ct [GAPDH]). We then averaged the resulting values for each sample over all expressing technical replicates. For clustering analysis, Cts then were normalized gene by gene by mean-centering and dividing by 3× the standard deviation (3 SD) of expressing cells as previously described.[59]

RNA-seq

Sequencing

Sequencing libraries were prepared using MARSeq. Single reads were sequenced on one lane of an Illumina NextSeq.

Bioinformatics

Poly(A/T) stretches and Illumina adapters were trimmed from the reads using cutadapt[55]; resulting reads shorter than 30 bp were discarded. Reads were mapped to the *Homo sapiens* reference genome GRCh38 using STAR,[56] supplied with gene annotations downloaded from Ensembl (and with EndToEnd option, and outFilterMismatchNoverLmax was set to 0.04). Expression levels for each gene were quantified using htseq-count,[57] using the gtf above.

Figure 7. OCT4-kSPH have the capacity to create tubular structures *in vivo*

(A) OCT4-kSPH (P7–P10) were injected into NOD-SCID mice with Matrigel. At day 14, tubule-like structures obtained from the injected cells (HLA^+) were evident (i–iii). (B) OCT4-kSPH-derived tubule-like structures were positively stained for cytokeratin, CD13, AQP1, LRP2, and LTL. (C) Similar structures developed from low-passage (P1) hKEpC-kSPH.

RNA-seq data analysis

Data normalization and differential gene expression were done by DESeq2.[58] R packages pheatmap and ggplot2 were used for data visualization. The GSEA tool was used to find gene sets that were enriched in two gene lists ranked by their log2 fold change ratio.[60] Ontology analysis was performed using ClusterProfiler[61] and visualized with GOplot.[62] We also performed gene enrichment analysis using ToppGene[63] and selected annotations related to kidney development, proliferation, structure, and function.

Overlap analysis

The GeneOverlap R package[64] was used to test for overlaps between ChIP-seq results and known HNF1B and OCT4 targets as well as between ChIP-seq results and RNA-seq results.

Chromatin immunoprecipitation

ChIP was performed as previously described.[65,66] In brief, 10 million cells were fixed with 1% formaldehyde for 10 min at room temperature, treated with 125 mM glycine for 5 min at room temperature, and washed three times with ice-cold PBS. The dry pellet was flash-frozen in liquid nitrogen. The pellet was resuspended in 0.5 mL SDS lysis buffer (1% SDS, 10 mM EDTA [pH 8], 50 mM Tris [pH 8.1]) and incubated for 30 min on ice. Chromatin was sheared to 200–500 bp with 30–35 cycles of 0.5 s ON/OFF using the Bioruptor sonicator (Diagenode). Chromatin from 2 million cells was diluted 1:10 in ChIP dilution buffer (1.1% Triton, 1.2 mM EDTA, 16.7 mM Tris-HCl [pH 8.1], 167 mM NaCl), immunoprecipitated overnight at 4°C with either H3K4me3 (2 μg; abcam; ab8580) or IgG (abcam; ab46540) antibodies along with Magna ChIP protein A magnetic beads (Merck Millipore; 16-661). Beads were harvested and sequentially washed for 2 min on a rotating platform with 1 mL of each of the following buffers: low-salt immune complex wash buffer (0.1% SDS, 1% Triton, 2 mM EDTA, 20 mM Tris [pH 8.1], 150 mM NaCl), high-salt immune complex buffer (0.1% SDS, 1% Triton, 2 mM EDTA, 20 mM Tris [pH 8.1], 500 mM NaCl), LiCl immune complex buffer (0.25 M LiCl, 1% NP-40, 1% deoxycholic acid, 1 mM EDTA, 10 mM Tris [pH 8.1]), and TE (10 mM Tris, 1 mM EDTA). Chromatin-antibody complexes were eluted using elution buffer (300 μL of 1% SDS, 1 mM EDTA, 10 mM Tris [pH 8.1], 200 mM NaCl). Samples were treated with RNase (0.5 h, 37°C). Crosslinking was reversed by incubation of the eluted samples overnight at 65°C with proteinase K. Samples were purified with phenol: chloroform and ethanol precipitation.

Library preparation was carried out as published.[67] Multiplexed libraries were sequenced on HiSeq2500 using 50 bp single-end read runs, generating for the following number of reads naive, H3K4me3_1 (20,983,419) and H3K4me3_2 (14,304,627), and OCT4, H3K4me3_1 (19,447,498) and H3K4me3_2 (25,383,337).

ChIP-seq analysis

ChIP-seq reads were aligned to the human GRCh37/hg19 genome assembly using Bowtie[68] with default settings. The average percentages of aligned reads were 89% for H3K4me3, for the naive, and 90% for the OCT4. Significant peaks of H3K4me3 were extracted using MACS 1.4,[67] using a minimal p value cutoff of 10^{-5} and a fold change for model building of 30. The density profiles of naive and OCT4 centered onto the TSS (transcription start site) of UCSC genes (±5 kb) were generated using SeqMiner. The sum of the reads in each bin was normalized by the total number of the aligned reads (31,699,326 and 40,433,586 reads for the naive and OCT4, respectively).

Cytogenetic analysis

Chromosome preparations were acquired according to standard procedures. The mitotic arrestant colcemid was added to the cell cultures, which were harvested following trypsinization. Slides were subsequently prepared from fixed (methanol:acetic acid 3:1) suspensions and, following aging, trypsin G banded and Giemsa stained. The subsequent cytogenetic analysis and interpretation were made according to ISCN 1995.[69]

NOD/SCID grafting

hKEpC, OCT4-hKEpC, or kSPH (1×10^6) were suspended within Matrigel (BD Biosciences) and were implanted into the SC space of 8- to 10-week-old NOD/SCID mice. Grafts were harvested 14 days (T14) after injection and fixed overnight in 4% buffered PFA and embedded in paraffin.

Integration test

cmDil-labeled hKEpC or OCT4-hKEpC were co-suspended with hFKCs (not labeled) within Matrigel and were implanted into the SC space of 8- to 10-week-old NOD/SCID mice. Fourteen days after injection, the grafts were harvested and immediately embedded into OCT medium (Sakura Finetek, CA) for frozen blocking.

Statistical analysis

Results are expressed as the mean values ± SD. Statistical differences between group data were compared by Student's t test. Where indicated, t test was performed after logarithmic transformation to achieve normality. For all statistical analyses, the level of significance was set as $p < 0.05$.

Data availability

The data supporting the studies presented in this article can be found in the main text or the supplemental information. Additional information may be made available upon reasonable request to the corresponding authors as appropriate.

SUPPLEMENTAL INFORMATION

Supplemental information can be found online at https://doi.org/10.1016/j.omtm.2023.04.005.

ACKNOWLEDGMENTS

We wish to thank Prof. Zohar Dotan from the Department of Urology, Sheba Medical Center, Tel Hashomer, for providing human kidney tissue samples. The work is supported by ISF (Israel Science Foundation) grants 910/11 and 2071/17, the Israel Ministry of

Industry "NOFAR" program, Wolfoson Clore Mayer, and the Sagol Center for Regenerative Medicine, School of Medicine, Tel Aviv University (B.D.); an NIH-NIDDK Diabetic Complications Pilot & Feasibility grant (DK076169), the NephroTools FP7 Marie Curie Initial Training Network (project 289754), and The Lisa and David Pulver Family Foundation (B.D.). E.M. is the Arthur Gutterman Family Chair for Stem Cell Research. This work was partially supported by a generous gift from Arthur Gutterman to E.M. and B.D.

AUTHOR CONTRIBUTIONS

D.O. conducted and designed the experiments and wrote the paper, O.H.-S. conducted and designed the experiments, O.C.Z. performed bioinformation analysis, O.P. wrote the paper, Y.G. performed experiments and analysis, M.N. performed experiments and analysis, A.-H.C. performed experiments and analysis, M.N.-R. performed experiments and analysis, G.T. performed experiments and analysis, T.K. designed experiments and analysis, E.M. designed experiments and wrote the paper, and B.D. conducted and designed the experiments and wrote the paper.

DECLARATION OF INTERESTS

The authors declare no competing interests.

REFERENCES

1. Matas, A.J., Adair, A., and Wigmore, S.J. (2011). The case for a regulated system of incentives for living kidney donation. Ann. R. Coll. Surg. Engl. *93*, 188–192. https://doi.org/10.1308/rcsann.2011.93.3.188a.
2. Metsuyanim, S., Pode-Shakked, N., Schmidt-Ott, K.M., Keshet, G., Rechavi, G., Blumental, D., and Dekel, B. (2008). Accumulation of malignant renal stem cells is associated with epigenetic changes in normal renal progenitor genes. Stem Cell. *26*, 1808–1817.
3. Harari-Steinberg, O., Metsuyanim, S., Omer, D., Gnatek, Y., Gershon, R., Pri-Chen, S., Ozdemir, D.D., Lerenthal, Y., Noiman, T., Ben-Hur, H., et al. (2013). Identification of human nephron progenitors capable of generation of kidney structures and functional repair of chronic renal disease. EMBO Mol. Med. *5*, 1556–1568.
4. Cohen-Zontag, O., Gershon, R., Harari-Steinberg, O., Kanter, I., Omer, D., Pleniceanu, O., Tam, G., Oriel, S., Ben-Hur, H., Katz, G., et al. (2020). Human kidney clonal proliferation disclose lineage-restricted precursor characteristics. Sci. Rep. *10*, 22097.
5. Harari-Steinberg, O., Pleniceanu, O., and Dekel, B. (2011). Selecting the optimal cell for kidney regeneration: fetal, adult or reprogrammed stem cells. Organogenesis *7*, 123–134.
6. Pleniceanu, O., Harari-Steinberg, O., and Dekel, B. (2010). Concise review: kidney stem/progenitor cells: differentiate, sort out, or reprogram? Stem Cell. *28*, 1649–1660.
7. Schutgens, F., and Clevers, H. (2019). Human organoids: tools for understanding biology and treating diseases. Annu. Rev. Pathol. *15*, 1–24. https://doi.org/10.1146/annurev-pathmechdis.
8. Freedman, B.S. (2015). Modeling kidney disease with iPS cells: supplementary issue: stem cell biology. Biomark. Insights *10*, 153–169.
9. Harari-Steinberg, O., Omer, D., Gnatek, Y., Pleniceanu, O., Goldberg, S., Cohen-Zontag, O., Pri-Chen, S., Kanter, I., Ben Haim, N., Becker, E., et al. (2020). Ex vivo expanded 3D human kidney spheres engraft long term and repair chronic renal injury in mice. Cell Rep. *30*, 852–869.e4.
10. Rinkevich, Y., Montoro, D.T., Contreras-Trujillo, H., Harari-Steinberg, O., Newman, A.M., Tsai, J.M., Lim, X., Van-Amerongen, R., Bowman, A., Januszyk, M., et al. (2014). *In Vivo* clonal analysis reveals lineage-restricted progenitor characteristics in mammalian kidney development, maintenance, and regeneration. Cell Rep. *7*, 1270–1283.
11. Chang-Panesso, M., Kadyrov, F.F., Lalli, M., Wu, H., Ikeda, S., Kefaloyianni, E., Abdelmageed, M.M., Herrlich, A., Kobayashi, A., and Humphreys, B.D. (2019). FOXM1 drives proximal tubule proliferation during repair from acute ischemic kidney injury. J. Clin. Invest. *129*, 5501–5517.
12. Lu, Y.-A., Liao, C.T., Raybould, R., Talabani, B., Grigorieva, I., Szomolay, B., Bowen, T., Andrews, R., Taylor, P.R., and Fraser, D. (2021). Single-nucleus RNA sequencing identifies new classes of proximal tubular epithelial cells in kidney fibrosis. J. Am. Soc. Nephrol. *32*, 2501–2516.
13. Young, M.D., Mitchell, T.J., Vieira Braga, F.A., Tran, M.G.B., Stewart, B.J., Ferdinand, J.R., Collord, G., Botting, R.A., Popescu, D.M., Loudon, K.W., et al. (2018). Single-cell transcriptomes from human kidneys reveal the cellular identity of renal tumors. Science *361*, 594–599.
14. Muto, Y., Wilson, P.C., Ledru, N., Wu, H., Dimke, H., Waikar, S.S., and Humphreys, B.D. (2021). Single cell transcriptional and chromatin accessibility profiling redefine cellular heterogeneity in the adult human kidney. Nat. Commun. *12*, 2190.
15. Schutgens, F., Rookmaaker, M.B., Margaritis, T., Rios, A., Ammerlaan, C., Jansen, J., Gijzen, L., Vormann, M., Vonk, A., Viveen, M., et al. (2019). Tubuloids derived from human adult kidney and urine for personalized disease modeling. Nat. Biotechnol. *37*, 303–313.
16. Little, M.H., and Bertram, J.F. (2009). Is there such a thing as a renal stem cell? J. Am. Soc. Nephrol. *20*, 2112–2117.
17. Szabo, E., Rampalli, S., Risueño, R.M., Schnerch, A., Mitchell, R., Fiebig-Comyn, A., Levadoux-Martin, M., and Bhatia, M. (2010). Direct conversion of human fibroblasts to multilineage blood progenitors. Nature *468*, 521–526.
18. Efe, J.A., Hilcove, S., Kim, J., Zhou, H., Ouyang, K., Wang, G., Chen, J., and Ding, S. (2011). Conversion of mouse fibroblasts into cardiomyocytes using a direct reprogramming strategy. Nat. Cell Biol. *13*, 215–222.
19. Kim, J., Efe, J.A., Zhu, S., Talantova, M., Yuan, X., Wang, S., Lipton, S.A., Zhang, K., and Ding, S. (2011). Direct reprogramming of mouse fibroblasts to neural progenitors. Proc. Natl. Acad. Sci. USA *108*, 7838–7843.
20. Sterneckert, J., Höing, S., and Schöler, H.R. (2012). Concise review: oct4 and more: the reprogramming expressway. Stem Cell. *30*, 15–21.
21. Babaie, Y., Herwig, R., Greber, B., Brink, T.C., Wruck, W., Groth, D., Lehrach, H., Burdon, T., and Adjaye, J. (2007). Analysis of Oct4-dependent transcriptional networks regulating self-renewal and pluripotency in human embryonic stem cells. Stem Cell. *25*, 500–510.
22. Loh, K.M., and Lim, B. (2011). A precarious balance: pluripotency factors as lineage specifiers. Cell Stem Cell *8*, 363–369.
23. Niwa, H., Miyazaki, J.i., and Smith, A.G. (2000). Quantitative expression of Oct-3/4 defines differentiation, dedifferentiation or self-renewal of ES cells. Nat. Genet. *24*, 372–376.
24. Hochedlinger, K., Yamada, Y., Beard, C., and Jaenisch, R. (2005). Ectopic expression of Oct-4 blocks progenitor-cell differentiation and causes dysplasia in epithelial tissues. Cell *121*, 465–477.
25. Buzhor, E., Omer, D., Harari-Steinberg, O., Dotan, Z., Vax, E., Pri-Chen, S., Metsuyanim, S., Pleniceanu, O., Goldstein, R.S., and Dekel, B. (2013). Reactivation of NCAM1 defines a subpopulation of human adult kidney epithelial cells with clonogenic and stem/progenitor properties. Am. J. Pathol. *183*, 1621–1633.
26. Buzhor, E., Harari-Steinberg, O., Omer, D., Metsuyanim, S., Jacob-Hirsch, J., Noiman, T., Dotan, Z., Goldstein, R.S., and Dekel, B. (2011). Kidney spheroids recapitulate tubular organoids leading to enhanced tubulogenic potency of human kidney-derived cells. Tissue Eng. Part A *17*, 2305–2319.
27. Reidy, K.J., and Rosenblum, N.D. (2009). Cell and molecular biology of kidney development. Semin. Nephrol. *29*, 321–337.
28. N, D.-P., J, Z., and D, D. (2007). Distinct roles and regulations for HoxD genes in metanephric kidney development. PLoS Genet. *3*, 2500–2514.
29. Lee, Y., Nadal-Ginard, B., Mahdavi, V., and Izumo, S. (1997). Myocyte-specific enhancer factor 2 and thyroid hormone receptor associate and synergistically activate the alpha-cardiac myosin heavy-chain gene. Mol. Cell Biol. *17*, 2745–2755.

30. North, T.E., de Bruijn, M.F.T.R., Stacy, T., Talebian, L., Lind, E., Robin, C., Binder, M., Dzierzak, E., and Speck, N.A. (2002). Runx1 expression marks long-term repopulating hematopoietic stem cells in the midgestation mouse embryo. Immunity *16*, 661–672.

31. Hochedlinger, K., Yamada, Y., Beard, C., and Jaenisch, R. (2005). Ectopic expression of Oct-4 blocks progenitor-cell differentiation and causes dysplasia in epithelial tissues. Cell *121*, 465–477.

32. Mukherjee, M., deRiso, J., Otterpohl, K., Ratnayake, I., Kota, D., Ahrenkiel, P., Chandrasekar, I., and Surendran, K. (2019). Endogenous Notch signaling in adult kidneys maintains segment-specific epithelial cell types of the distal tubules and collecting ducts to ensure water homeostasis. J. Am. Soc. Nephrol. *30*, 110–126.

33. Oki, S., Ohta, T., Shioi, G., Hatanaka, H., Ogasawara, O., Okuda, Y., Kawaji, H., Nakaki, R., Sese, J., and Meno, C. (2018). ChIP-Atlas: a data-mining suite powered by full integration of public ChIP-seq data. EMBO Rep. *19*.

34. Sanulli, S., Justin, N., Teissandier, A., Ancelin, K., Portoso, M., Caron, M., Michaud, A., Lombard, B., da Rocha, S.T., Offer, J., et al. (2015). Jarid2 methylation via the PRC2 complex regulates H3K27me3 deposition during cell differentiation. Mol. Cell *57*, 769–783.

35. Desgrange, A., Heliot, C., Skovorodkin, I., Akram, S.U., Heikkilä, J., Ronkainen, V.P., Miinalainen, I., Vainio, S.J., and Cereghini, S. (2017). HNF1B controls epithelial organization and cell polarity during ureteric bud branching and collecting duct morphogenesis. Development *144*, 4704–4719.

36. Paces-Fessy, M., Fabre, M., Lesaulnier, C., S, C., and Cereghini, S. (2012). Hnf1b and Pax2 cooperate to control different pathways in kidney and ureter morphogenesis. Hum. Mol. Genet. *21*, 3143–3155.

37. Heliot, C., Desgrange, A., Buisson, I., Prunskaite-Hyyryläinen, R., Shan, J., Vainio, S., Umbhauer, M., and Cereghini, S. (2013). HNF1B controls proximal-intermediate nephron segment identity in vertebrates by regulating Notch signalling components and Irx1/2. Development *140*, 873–885.

38. Chan, S.C., Zhang, Y., Shao, A., Avdulov, S., Herrera, J., Aboudehen, K., Pontoglio, M., and Igarashi, P. (2018). Mechanism of fibrosis in HNF1B-related autosomal dominant tubulointerstitial kidney disease. J. Am. Soc. Nephrol. *29*, 2493–2509.

39. Wang, J., He, C., Gao, P., Wang, S., Lv, R., Zhou, H., Zhou, Q., Zhang, K., Sun, J., Fan, C., et al. (2020). HNF1B-mediated repression of SLUG is suppressed by EZH2 in aggressive prostate cancer. Oncogene *39*, 1335–1346.

40. Harikumar, A., and Meshorer, E. (2015). Chromatin remodeling and bivalent histone modifications in embryonic stem cells. EMBO Rep. *16*, 1609–1619.

41. Metsuyanim, S., Harari-Steinberg, O., Buzhor, E., Omer, D., Pode-Shakked, N., Ben-Hur, H., Halperin, R., Schneider, D., and Dekel, B. (2009). Expression of stem cell markers in the human fetal kidney. PLoS One *4*, e6709.

42. Dominici, M., Le Blanc, K., Mueller, I., Slaper-Cortenbach, I., Marini, F., Krause, D., Deans, R., Keating, A., Prockop, D., and Horwitz, E. (2006). Minimal criteria for defining multipotent mesenchymal stromal cells. The International Society for Cellular Therapy position statement. Cytotherapy *8*, 315–317.

43. Kim, S.S., Gwak, S.J., Han, J., Park, H.J., Park, M.H., Song, K.W., Cho, S.W., Rhee, Y.H., Chung, H.M., and Kim, B.S. (2007). Kidney tissue reconstruction by fetal kidney cell transplantation: effect of gestation stage of fetal kidney cells. Stem Cell. *25*, 1393–1401.

44. Bhargava, P., and Schnellmann, R.G. (2017). Mitochondrial energetics in the kidney. Nat. Rev. Nephrol. *13*, 629–646.

45. Bataille, A., Galichon, P., Chelghoum, N., Oumoussa, B.M., Ziliotis, M.J., Sadia, I., Vandermeersch, S., Simon-Tillaux, N., Legouis, D., Cohen, R., et al. (2018). Increased fatty acid oxidation in differentiated proximal tubular cells surviving a reversible episode of acute kidney injury. Cell. Physiol. Biochem. *47*, 1338–1351.

46. Kang, H.M., Ahn, S.H., Choi, P., Ko, Y.A., Han, S.H., Chinga, F., Park, A.S.D., Tao, J., Sharma, K., Pullman, J., et al. (2015). Defective fatty acid oxidation in renal tubular epithelial cells has a key role in kidney fibrosis development. Nat. Med. *21*, 37–46.

47. Omer, D., Harari-Steinberg, O., Buzhor, E., Metsuyanim, S., Pleniceanu, O., Zundelevich, A., Gal-Yam, E.N., and Dekel, B. (2013). Chromatin-modifying agents reactivate embryonic renal stem/progenitor genes in human adult kidney epithelial cells but abrogate dedifferentiation and stemness. Cell. Reprogram. *15*, 281–292.

48. Park, J.S., Ma, W., O'Brien, L.L., Chung, E., Guo, J.J., Cheng, J.G., Valerius, M.T., McMahon, J.A., Wong, W.H., and McMahon, A.P. (2012). Six2 and Wnt regulate self-renewal and commitment of nephron progenitors through shared gene regulatory networks. Dev. Cell *23*, 637–651.

49. Omer, D., Pleniceanu, O., Gnatek, Y., Namestnikov, M., Cohen-Zontag, O., Goldberg, S., Friedman, Y.E., Friedman, N., Mandelboim, M., Vitner, E.B., et al. (2021). Human kidney spheroids and monolayers provide insights into SARS-CoV-2 renal interactions. J. Am. Soc. Nephrol. *32*, 2242–2254.

50. Takasato, M., Er, P.X., Chiu, H.S., Maier, B., Baillie, G.J., Ferguson, C., Parton, R.G., Wolvetang, E.J., Roost, M.S., Lopes, S.M.C.d.S., and Little, M.H. (2016). Kidney organoids from human iPS cells contain multiple lineages and model human nephrogenesis. Nature *536*, 238.

51. Sander, V., Salleh, L., Naylor, R.W., Schierding, W., Sontam, D., O'Sullivan, J.M., and Davidson, A.J. (2019). Transcriptional profiling of the zebrafish proximal tubule. Am. J. Physiol. Renal Physiol. *317*, F478–F488.

52. RA, G., et al. (2015). Genome-wide studies reveal that H3K4me3 modification in bivalent genes is dynamically regulated during the pluripotent cell cycle and stabilized upon differentiation. Mol. Cell Biol. *36*, 615–627.

53. Lakkaraju, A., Finnemann, S.C., and Rodriguez-Boulan, E. (2007). The lipofuscin fluorophore A2E perturbs cholesterol metabolism in retinal pigment epithelial cells. Proc. Natl. Acad. Sci. USA *104*, 11026–11031.

54. Kaminski, M.M., Tosic, J., Kresbach, C., Engel, H., Klockenbusch, J., Müller, A.L., Pichler, R., Grahammer, F., Kretz, O., Huber, T.B., et al. (2016). Direct reprogramming of fibroblasts into renal tubular epithelial cells by defined transcription factors. Nat. Cell Biol. *18*, 1269–1280.

55. Kechin, A., Boyarskikh, U., Kel, A., and Filipenko, M. (2017). A new tool for accurate cutting of primers from reads of targeted next generation sequencing. J. Comput. Biol. *24*, 1138–1143.

56. Dobin, A., Davis, C.A., Schlesinger, F., Drenkow, J., Zaleski, C., Jha, S., Batut, P., Chaisson, M., and Gingeras, T.R. (2013). STAR: ultrafast universal RNA-seq aligner. Bioinformatics *29*, 15–21.

57. Anders, S., Pyl, P.T., and Huber, W. (2015). HTSeq–a Python framework to work with high-throughput sequencing data. Bioinformatics *31*, 166–169.

58. Love, M.I., Huber, W., and Anders, S. (2014). Moderated estimation of fold change and dispersion for RNA-seq data with DESeq2. Genome Biol. *15*, 550–621.

59. Dalerba, P., Kalisky, T., Sahoo, D., Rajendran, P.S., Rothenberg, M.E., Leyrat, A.A., Sim, S., Okamoto, J., Johnston, D.M., Qian, D., et al. (2011). Single-cell dissection of transcriptional heterogeneity in human colon tumors. Nat. Biotechnol. *29*, 1120–1127.

60. Subramanian, A., Tamayo, P., Mootha, V.K., Mukherjee, S., Ebert, B.L., Gillette, M.A., Paulovich, A., Pomeroy, S.L., Golub, T.R., et al. (2005). Gene set enrichment analysis: a knowledge-based approach for interpreting genome-wide expression profiles. Proc. Natl. Acad. Sci. USA *102*, 15545–15550.

61. Guangchuang, Y., Li-Gen, W., Yanyan, H., and Qing-Yu, H. (2012). An R package for comparing biological themes among gene clusters. OMICS *16*, 284–287.

62. Walter, W., Sánchez-Cabo, F., and Ricote, M. (2015). An R package for visually combining expression data with functional analysis. Bioinformatics *31*, 2912–2914.

63. Chen, J., Bardes, E.E., Aronow, B.J., and Jegga, A.G. (2009). ToppGene Suite for gene list enrichment analysis and candidate gene prioritization. Nucleic Acids Res. *37*, W305–W311.

64. (2013). Bioconductor - GeneOverlap. https://bioconductor.org/packages/release/bioc/html/GeneOverlap.html.

65. Hezroni, H., Tzchori, I., Davidi, A., Mattout, A., Biran, A., Nissim-Rafinia, M., Westphal, H., and Meshorer, E. (2011). H3K9 histone acetylation predicts pluripotency and reprogramming capacity of ES cells. Nucleus *2*, 300–309.

66. Sailaja, B.S., Cohen-Carmon, D., Zimmerman, G., Soreq, H., E, M., and Meshorer, E. (2012). Stress-induced epigenetic transcriptional memory of acetylcholinesterase by HDAC4. Proc. Natl. Acad. Sci. USA *109*, E3687–E3695.

67. Zhang, Y., Liu, T., Meyer, C.A., Eeckhoute, J., Johnson, D.S., Bernstein, B.E., Nusbaum, C., Myers, R.M., Brown, M., Li, W., and Liu, X.S. (2008). Model-based analysis of ChIP-seq (MACS). Genome Biol. *9*, R137.

68. Langmead, B., Trapnell, C., Pop, M., and Salzberg, S.L. (2009). Ultrafast and memory-efficient alignment of short DNA sequences to the human genome. Genome Biol. *10*, R25.

69. International Standing Committee on Human Cytogenetic Nomenclature, and Mitelman, F. (1995). ISCN 1995 : An International System for Human Cytogenetic Nomenclature. In Recommendations of the International Standing Committee on Human Cytogenetic Nomenclature, Memphis, Tennessee, USA, October 9-13, 1994, p. 114.